Eur. Phys. J. Plus (2025) 140:802
https://doi.org/10.1140/epjp/s13360-025-06630-4

THE EUROPEAN PHYSICAL JOURNAL PLUS

Regular Article

# Dirac equation solution with generalized tanh-shaped hyperbolic potential: application to charmonium and bottomonium mass spectra

**V. H. Badalov**[1,2,a], **A. I. Ahmadov**[1,3], **E. A. Dadashov**[4], **S. V. Badalov**[5,6,b]

[1] Institute for Physical Problems, Baku State University, AZ-1148 Baku, Azerbaijan
[2] Center for Theoretical Physics, Khazar University, AZ-1096 Baku, Azerbaijan
[3] Department of Theoretical Physics, Baku State University, AZ-1148 Baku, Azerbaijan
[4] Department of Chemistry and Physics, Lankaran State University, AZ-4200 Lankaran, Azerbaijan
[5] Department of Physics, University of Bayreuth, 95447 Bayreuth, Germany
[6] Bavarian Center for Battery Technologies, University of Bayreuth, 95448 Bayreuth, Germany

Received: 15 March 2025 / Accepted: 7 July 2025


**Abstract** In this study, we present an analytical solution of the Dirac equation in a generalized tanh-shape hyperbolic potential, which allows us to unify various well-known quantum potentials under a single theoretical framework. This versatile potential model is used to compute the mass spectra for charmonium and bottomonium, with excellent agreement with experimental measurements, and does better than some potential models in predicting the several orbital states. Our results not only validate the GTHP as a powerful tool for describing heavy quarkonium systems but also suggest its broader applicability in exploring quantum systems where similar potentials are effective. This work is a stepping stone for new research into fermionic systems with complex interactions, by jointly providing insights into foundational aspects of quantum mechanics as well as applications in particle physics.

## 1 Introduction

The Dirac equation (DE) is a cornerstone of quantum mechanics and is responsible for revolutionizing theoretical physics, giving rise to what is in essence the first relativistic quantum field theory, leading to the prediction of novel phenomena such as antimatter [1]. The equation has led to advances in many areas in physics, from quantum electrodynamics [2] to the way particles behave in the relativistic limit [3, 4]. Responsible in its particular nuclear properties studies [5], which later extended to be used in potent modern effort in a superheavy element [6], complex quantum systems [7], chiral symmetric quantum chromodynamics [8] and antiparticles [9]. In addition, DE continues to be relevant for current research and opens the possibility to study electron vortices [10], coherent control [11] and new theoretical approaches [12–16].

The DE is at the core of the concepts of spin and pseudo-spin symmetries, which are embedded within the Dirac Hamiltonian [17–26]. They explain a variety of physical phenomena associated with the simplicial background and are definitive tools in the interpretation of nuclear structure and reactions [18–23]. Spin symmetry, manifesting as a spin doublet, leads to degeneracy between states characterized by quantum numbers $(n,\ l,\ j = l \pm s)$ [20–23]. This symmetry is instrumental in elucidating the spectrum of antinucleons in a nucleus and the subtle spin-orbit splitting observed in hadrons [24]. In contrast, pseudo-spin symmetry, another form of degeneracy, arises between states with quantum numbers $(n,\ l,\ j = l+\frac{1}{2})$ and $(n-1,\ l+2,\ j = l+\frac{3}{2})$ [25, 26]. This symmetry has profound implications for understanding nuclear deformation [27, 28], identical bands [29–31], magnetic moments [32, 33], magic number shifts [34–36] and effective shell-model structures in nuclear physics [37].

Pseudo-spin symmetry was initially explored within the non-relativistic framework and later extended into relativistic mean field theory [24, 25]. Significant strides have been made in this domain, with comprehensive investigations revealing the intricate details of spin and pseudo-spin symmetries [21, 22, 38]. Significant advancements have been made in this area, particularly through the analytical solutions of the DE with physical potentials, which are crucial for uncovering the full spectrum of a quantum system's properties [39–42]. In this context, our focus is on solving the DE for the generalized tanh-shaped hyperbolic potential (GTHP) [43, 44], described as:

$$V(r) = V_1 + V_2 \tanh(\alpha r) + V_3 \tanh^2(\alpha r), \tag{1}$$

[a] e-mail: badalovvatan@yahoo.com
[b] e-mail: sabuhi.badalov@uni-bayreuth.de (corresponding author)

Published online: 26 August 2025

where $V_1$, $V_2$, and $V_3$ represent potential well depths, and $\alpha$ characterizes the interaction potential's properties. The GTHP exhibits a minimum value $V_{\min} = V(r_e) = V_1 - \frac{V_2^2}{4V_3}$ at $r_e = \frac{1}{\alpha}\tanh^{-1}\left(-\frac{V_2}{2V_3}\right)$, subject to $|V_2| < 2V_3$ and $V_3 > 0$ [43, 44]. This potential encompasses a wide range of physical scenarios, including various standard and generalized potential models, including the standard and generalized Woods–Saxon [17, 45, 46], Rosen–Morse [47], Manning–Rosen type [48], standard and generalized Morse (improved Rosen–Morse) [49, 50], Schiöberg [51, 52], four-parametric exponential type [53, 54], Williams–Poulios [55, 56], and the sum of the linear and harmonic oscillator potentials in some special cases [43, 44]. Notably, considering $V_1 \neq 0$ in GTHP facilitates the modeling of these particular cases [43, 44]. These potentials are particularly relevant in modeling complex quantum systems, where the GTHP's flexibility allows it to capture a broad spectrum of interactions.

While previous studies have significantly advanced our understanding of so-called spin symmetries in relativistic and non-relativistic fields and clarified the critical spin dynamics, there is still a significant gap in applying these insights to complex potentials that more accurately reflect real quantum phenomena. With this study, we aim to fill this gap by advancing our understanding of the hadronic physics and GTHP. This work investigates the bound-state solutions of the DE from the perspective of the GTHP. Employing the Nikiforov–Uvarov (NU) method, reducing the second-order differential equation to a hypergeometric form, we derive exact expressions for the energy eigenvalues and the corresponding radial wave functions articulated through hypergeometric polynomials for various quantum states. Our analysis reveals the sensitivity of these eigenvalues to variations in the potential parameters, providing deep insights into the quantum dynamics encapsulated by the GTHP model. Furthermore, we extend our theoretical framework to studying heavy quark systems, specifically targeting the charmonium and bottomonium mass spectra. Heavy quarkonia, consisting of a heavy quark and antiquark (such as $b\bar{b}$ and $c\bar{c}$), serve as a critical testing ground for quantum chromodynamics (QCD) and various potential models [57–67]. These systems are particularly significant owing to their rich spectroscopy, with many states lying below the threshold of open charm or bottom production [16, 60–76]. Employing the GTHP model to these systems, one is able to extract bound-state masses with quite good agreement with experimental results leading to important knowledge on heavy quark interaction dynamics and properties of quark–antiquark potentials on hadronic scales.

To facilitate a comprehensive understanding of the findings, this paper is structured as follows: Sect. 2 presents the bound-state solution of the radial DE for GTHP using the NU method. In Sect. 3, we discuss the results for energy levels in specific cases, and the mass spectrum analyses for the $b\bar{b}$ and $c\bar{c}$ systems. Concluding remarks and implications of our study are outlined in Sect. 4.

## 2 Solutions to the radial dirac equation

The DE serves as a fundamental framework for describing the quantum behavior of fermions in the presence of scalar and vector potentials [77]. For a particle interacting with an attractive scalar potential $S(\vec{r})$ and a repulsive vector potential $V(\vec{r})$, the DE is given by:

$$\left[c\vec{\alpha}\cdot\hat{\vec{p}} + \beta\big(Mc^2 + S(\vec{r})\big) + V(\vec{r})\right]\psi(\vec{r}) = E\psi(\vec{r}), \tag{2}$$

where $E$ is the relativistic total energy, $\hat{\vec{p}} = -i\hbar\vec{\nabla}$ is the momentum operator, and $\vec{\alpha}$ and $\beta$ are the standard Dirac matrices [77]. To study the system under the influence of the GTHP, we recast the DE into its radial form, exploiting spherical symmetry. In this context, both potentials $S(r)$ and $V(r)$ are functions of the radial coordinate $r$, which allows us to decompose the Dirac spinor into radial and angular parts. Consequently, the DE simplifies to coupled radial second-order linear differential equations for the upper and lower components of the wave function. This formalism is particularly efficient for investigating energy eigenvalues and wave functions in spherically symmetric potentials. Then, we applied NU method [78] to solve this radial second-order linear differential equations, see the derivation which is discussed detailed in Ref. [79]. The transition to a radial form is crucial as it highlights the symmetries inherent in DE, especially when analyzing the effects of scalar and vector potentials that vary only with radial distance. By effectively isolating the radial components, this approach facilitates a focused study of the impact of potential variations under global symmetries on fermionic behavior.

For spin and pseudo-spin symmetry cases, the corresponding energy eigenvalues $E_{\rm nk}$ and normalized radial wave functions are derived. The details of these derivations are discussed in Ref. [79], where specific symmetry conditions simplify the DE, such as $\Delta(r) = C_s$ for spin symmetry and $\Sigma(r) = C_{\rm ps}$ for pseudo-spin symmetry.

***Spin Symmetry Case***:
In the case of spin symmetry, $\frac{d\Delta(r)}{\rm dr} = 0$ leads to the condition $\Delta(r) = C_s$. This simplifies the DE, and the energy eigenvalues $E_{\rm nk}$ are obtained as follows:

$$\begin{aligned}
&\left(\mathrm{Mc}^2 - C_s\right)^2 - E_{\mathrm{nk}}^2 + \left(\mathrm{Mc}^2 + E_{\mathrm{nk}} - C_s\right)(V_1 + V_2 + V_3) \\
&\quad + \frac{\hbar^2 c^2 k(k+1)}{r_e^2}(A_0 + A_1 + A_2) \\
&= \alpha^2\hbar^2 c^2 \left( \sqrt{\frac{1}{4} + \frac{\left(\mathrm{Mc}^2 + E_{\mathrm{nk}} - C_s\right)V_3}{\alpha^2\hbar^2 c^2} + \frac{k(k+1)}{\alpha^2 r_e^2} A_2} - n - \frac{1}{2} \right. \\
&\quad \left. + \frac{\frac{\left(\mathrm{Mc}^2 + E_{\mathrm{nk}} - C_s\right)V_2}{2\alpha^2\hbar^2 c^2} + \frac{k(k+1)}{2\alpha^2 r_e^2} A_1}{\sqrt{\frac{1}{4} + \frac{\left(\mathrm{Mc}^2 + E_{\mathrm{nk}} - C_s\right)V_3}{\alpha^2\hbar^2 c^2} + \frac{k(k+1)}{\alpha^2 r_e^2} A_2} - n - \frac{1}{2}} \right)^2 .
\end{aligned} \tag{3}$$

The information about all parameters in Eq. (3) and the full derivation process to obtain Eq. (3) are provided in Section S1 of Ref. [79].

***Pseudo-spin Symmetry Case***:
For pseudo-spin symmetry, $\frac{d\Sigma(r)}{\mathrm{dr}} = 0$ results in $\Sigma(r) = C_{\mathrm{ps}}$, which similarly simplifies the DE. The corresponding energy eigenvalues $E_{\mathrm{nk}}$ are expressed as:

$$\begin{aligned}
&\left(\mathrm{Mc}^2 + C_{\mathrm{ps}}\right)^2 - E_{\mathrm{nk}}^2 - \left(Mc^2 - E_{\mathrm{nk}} + C_{\mathrm{ps}}\right)(V_1 + V_2 + V_3) \\
&\quad + \frac{\hbar^2 c^2 k(k-1)}{r_e^2}(A_0 + A_1 + A_2) \\
&= \alpha^2\hbar^2 c^2 \left( \sqrt{\frac{1}{4} - \frac{(\mathrm{Mc}^2 - E_{\mathrm{nk}} + C_{\mathrm{ps}})V_3}{\alpha^2\hbar^2 c^2} + \frac{k(k-1)}{\alpha^2 r_e^2} A_2} - n - \frac{1}{2} \right. \\
&\quad \left. + \frac{-\frac{(\mathrm{Mc}^2 - E_{\mathrm{nk}} + C_{\mathrm{ps}})V_2}{2\alpha^2\hbar^2 c^2} + \frac{k(k-1)}{2\alpha^2 r_e^2} A_1}{\sqrt{\frac{1}{4} - \frac{(\mathrm{Mc}^2 - E_{\mathrm{nk}} + C_{\mathrm{ps}})V_3}{\alpha^2\hbar^2 c^2} + \frac{k(k-1)}{\alpha^2 r_e^2} A_2} - n - \frac{1}{2}} \right)^2 .
\end{aligned} \tag{4}$$

The information about all parameters in Eq. (4) and the full derivation process to obtain Eq. (4) are provided in Section S1 of Ref. [79].

While the current study is based on the NU method, we would like to note that recent developments in gauge theory and quantum integrability offer alternative frameworks for exact spectral analysis. For example, gauge theory approaches using the ordinary differential equation/integrable model correspondences have been applied to solve eigenvalue problems in $N = 2$ supersymmetric systems [80, 81]. Similarly, quantum integrability techniques based on functional Bethe *ansatz* equations have provided exact quantization conditions in contexts such as black hole quasi-normal mode spectra [82, 83]. These advances, including new exact solutions in supersymmetric gauge theory and gravity contexts, highlight the power of integrability-based methods and point to promising directions for extending the current model.

## 3 Results and discussion

### 3.1 Investigation of Spin Symmetry Case in Specific Scenarios

The GTHP is a highly versatile framework that exhibits a remarkable sensitivity to its parameters, making it an effective model to describe several prominent potentials encountered in fundamental quantum systems. The parametric flexibility of GTHP allows it to emulate various well-known potentials, such as the generalized Woods–Saxon [45, 46], Rosen–Morse [47], and Manning–Rosen potentials [48], among others. This adaptability stems from the intricate control of key parameters, such as $V_1$, $V_2$, $V_3$, and $\alpha$, which dictate the potential's shape, depth, and range.

It is well known that spin symmetry occurs in the DE when the difference between the vector and scalar potentials is constant, $V(r) - S(r) =$ constant. In this regime, the spin-orbit coupling becomes negligible, leading to near-degenerate energy levels and simplifying the relativistic energy spectrum [18, 19]. The ability to smoothly transition between different potential profiles by tuning these parameters makes GTHP an ideal model for exploring the underlying physics of systems with spin symmetry. Each set of parameters generates a distinct potential landscape, which strongly influences the system's energy levels, the degree of degeneracy, and the manifestation of spin symmetry. This symmetry is significant in high-energy physics and nuclear physics, particularly in

understanding mesonic and baryonic spectra, as well as nucleon–nucleon interactions. The sensitivity of GTHP model is also crucial for tailoring specific quantum systems and analyzing the behavior of relativistic particles in various physical environments as well as allowing for the emulation of short-range and long-range interactions across various fields of fundamental physics. We now examine the energy eigenvalue derived from Eq. (3) for different potentials modeled under the GTHP framework.

**i)** For the GTHP, selecting parameters $V_1 = -\frac{V_0}{2} - \frac{W}{4}$, $V_2 = \frac{V_0}{2}$, $V_3 = \frac{W}{4}$, and $\alpha = \frac{1}{2a}$ yields the following relation for the energy levels equation of the generalized Woods–Saxon potential:

$$\begin{aligned}
&\left(\mathrm{Mc}^2 - C_s\right)^2 - E_{\mathrm{nk}}^2 + \frac{\hbar^2 c^2 k(k+1)}{R_0^2} C_0 \\
&= \frac{\hbar^2 c^2}{4a^2}\left(\sqrt{\frac{1}{4} + \frac{(\mathrm{Mc}^2 + E_{nk} - C_s)a^2 W}{\hbar^2 c^2} + \frac{k(k+1)a^2}{R_0^2} C_2} - n - \frac{1}{2}\right. \\
&\left. + \frac{\frac{(\mathrm{Mc}^2+E_{nk}-C_s)a^2 V_0}{\hbar^2 c^2} - \frac{k(k+1)a^2}{R_0^2}(C_1 + C_2)}{\sqrt{\frac{1}{4} + \frac{(\mathrm{Mc}^2+E_{nk}-C_s)a^2 W}{\hbar^2 c^2} + \frac{k(k+1)a^2}{R_0^2} C_2} - n - \frac{1}{2}}\right)^2,
\end{aligned} \tag{5}$$

where $n = 0, 1, 2, \cdots n_{\max}$, and the energy levels are determined by the floor function of the square root expressions within the equation, incorporating the parameters $C_0$, $C_1$, and $C_2$ defined as follows:

$$\begin{aligned}
C_0 &= \frac{A_0 + A_1 + A_2}{(1 + x_e)^2}, \\
C_1 &= -\frac{2(A_1 + 2A_2)}{(1 + x_e)^2}, \\
C_2 &= \frac{4A_2}{(1 + x_e)^2},
\end{aligned} \tag{6}$$

with $x_e = \frac{r_e - R_0}{R_0}$. In here, $x_e$ represents a dimensionless variable that controls the shape of the potential.

**ii)** Considering the case when $W = 0$ and $x_e = 0$ for the energy levels equation of the standard Woods–Saxon potential [84], we derive:

$$\begin{aligned}
&\left(\mathrm{Mc}^2 - C_s\right)^2 - E_{\mathrm{nk}}^2 + \frac{\hbar^2 c^2 k(k+1)}{R_0^2} C_0 \\
&= \frac{\hbar^2 c^2}{4a^2}\left(\sqrt{\frac{1}{4} + \frac{k(k+1)a^2}{R_0^2} C_2} - n - \frac{1}{2} + \frac{\frac{(\mathrm{Mc}^2+E_{\mathrm{nk}}-C_s)a^2 V_0}{\hbar^2 c^2} - \frac{k(k+1)a^2}{R_0^2}(C_1 + C_2)}{\sqrt{\frac{1}{4} + \frac{k(k+1)a^2}{R_0^2} C_2} - n - \frac{1}{2}}\right)^2,
\end{aligned} \tag{7}$$

where $n = 0, 1, 2, \cdots n_{\max}$, and the coefficients $C_0$, $C_1$, and $C_2$ are adjusted accordingly to account for the absence of the $W$ and $x_e$ parameters.

**iii)** For the energy spectrum equation of the Rosen–Morse potential with parameters $V_3 = -V_1 = C$ and $V_2 = B$, the formulation is as follows:

$$\begin{aligned}
&\left(\mathrm{Mc}^2 - C_s\right)^2 - E_{\mathrm{nk}}^2 + (\mathrm{Mc}^2 + E_{\mathrm{nk}} - C_s)B + \frac{\hbar^2 c^2 k(k+1)}{r_e^2}(A_0 + A_1 + A_2) \\
&= \alpha^2 \hbar^2 c^2 \left(\sqrt{\frac{(\mathrm{Mc}^2 + E_{\mathrm{nk}} - C_s)C}{\alpha^2 \hbar^2 c^2} + \frac{k(k+1)}{\alpha^2 r_e^2} A_2 + \frac{1}{4}}\right. \\
&\left. - n - \frac{1}{2} + \frac{\frac{(\mathrm{Mc}^2+E_{\mathrm{nk}}-C_s)B}{2\alpha^2 \hbar^2 c^2} + \frac{k(k+1)}{2\alpha^2 r_e^2} A_1}{\sqrt{\frac{(\mathrm{Mc}^2+E_{\mathrm{nk}}-C_s)C}{\alpha^2 \hbar^2 c^2} + \frac{k(k+1)}{\alpha^2 r_e^2} A_2 + \frac{1}{4}} - n - \frac{1}{2}}\right)^2,
\end{aligned} \tag{8}$$

where $n = 0, 1, 2, \cdots n_{\max}$, signifying the quantum number associated with the energy level derived from the equation parameters and conditions.

**iv)** Incorporating the parameters of the GTHP for the Manning–Rosen type-potential, specifically $V_1 = \frac{\beta(\beta-1)-2A}{4\mathrm{kb}^2}$, $V_2 = -\frac{\beta(\beta-1)-A}{2\mathrm{kb}^2}$, $V_3 = \frac{\beta(\beta-1)}{4\mathrm{kb}^2}$, with $k = \frac{2M}{\hbar^2}$ and $2\alpha = \frac{1}{b}$, leads to the following formulation:

$$\begin{aligned}
&\left(\mathrm{Mc}^2 - C_s\right)^2 - E_{\mathrm{nk}}^2 + \frac{\hbar^2 c^2 k(k+1)}{r_e^2}(A_0 + A_1 + A_2) \\
&= \frac{\hbar^2 c^2}{4b^2}\left(\sqrt{\frac{1}{4} + \frac{(\mathrm{Mc}^2 + E_{\mathrm{nk}} - C_s)\beta(\beta-1)}{2\mathrm{Mc}^2} + \frac{4k(k+1)b^2}{r_e^2}A_2} - n - \frac{1}{2}\right. \\
&\left. + \frac{-\frac{(\mathrm{Mc}^2+E_{\mathrm{nk}}-C_s)[\beta(\beta-1)-A]}{2\alpha^2\hbar^2c^2} + \frac{2k(k+1)b^2}{r_e^2}A_1}{\sqrt{\frac{1}{4} + \frac{(\mathrm{Mc}^2+E_{\mathrm{nk}}-C_s)\beta(\beta-1)}{2\mathrm{Mc}^2} + \frac{4k(k+1)b^2}{r_e^2}A_2} - n - \frac{1}{2}}\right)^2,
\end{aligned} \tag{9}$$

where $n = 0, 1, 2, \ldots n_{\max}$, and the energy levels are evaluated using the complex interplay between the potential parameters and the quantum mechanical properties of the system.

**v)** By meticulously selecting the parameters within the GTHP framework, namely, $V_1 = \frac{1}{4}D_e(b-2)^2$, $V_2 = -\frac{1}{2}D_e b(b-2)$, $V_3 = \frac{1}{4}D_e b^2$, $2\alpha = \delta$ and $b = e^{\delta r_e} + 1 > 2$, we refine the approach to dissect the energy spectrum equation pertinent to the improved Rosen–Morse potential:

$$\begin{aligned}
&\left(\mathrm{Mc}^2 - C_s\right)^2 - E_{\mathrm{nk}}^2 + \left(\mathrm{Mc}^2 + E_{\mathrm{nk}} - C_s\right)D_e + \frac{\hbar^2 c^2 k(k+1)}{r_e^2}(A_0 + A_1 + A_2) \\
&= \frac{\delta^2\hbar^2c^2}{4}\left(\sqrt{\frac{1}{4} + \frac{(\mathrm{Mc}^2 + E_{\mathrm{nk}} - C_s)D_e b^2}{\delta^2\hbar^2c^2} + \frac{4k(k+1)}{\delta^2 r_e^2}A_2} - n - \frac{1}{2}\right. \\
&\left. - \frac{\frac{(\mathrm{Mc}^2+E_{\mathrm{nk}}-C_s)D_e b(b-2)}{\delta^2\hbar^2c^2} - \frac{2k(k+1)}{\delta^2 r_e^2}A_1}{\sqrt{\frac{1}{4} + \frac{(\mathrm{Mc}^2+E_{\mathrm{nk}}-C_s)b^2 D_e}{\delta^2\hbar^2c^2} + \frac{4k(k+1)}{\delta^2 r_e^2}A_2} - n - \frac{1}{2}}\right)^2.
\end{aligned} \tag{10}$$

The quantum numbers are denoted by $n = 0, 1, 2, \ldots n_{\max}$.

**vi)** Transitioning to the analysis of the Schiöberg potential, we adopt a nuanced parametrization: $V_1 = \delta^2 D$, $V_2 = -2\delta\sigma D$ and $V_3 = \sigma^2 D$. This setup facilitates the derivation of the energy spectrum equation, articulated as follows:

$$\begin{aligned}
&\left(\mathrm{Mc}^2 - C_s\right)^2 - E_{\mathrm{nk}}^2 + \left(\mathrm{Mc}^2 + E_{\mathrm{nk}} - C_s\right)(\delta-\sigma)^2 D + \frac{\hbar^2 c^2 k(k+1)}{r_e^2}C_0 \\
&= \alpha^2\hbar^2c^2\left(\sqrt{\frac{1}{4} + \frac{(\mathrm{Mc}^2 + E_{\mathrm{nk}} - C_s)\sigma^2 D}{\alpha^2\hbar^2c^2} + \frac{k(k+1)}{4\alpha^2 r_e^2}C_2}\right. \\
&\left. - n - \frac{1}{2} - \frac{\frac{(\mathrm{Mc}^2+E_{\mathrm{nk}}-C_s)\delta\sigma D}{\alpha^2\hbar^2c^2} - \frac{k(k+1)}{4\alpha^2 r_e^2}(C_1 - C_2)}{\sqrt{\frac{1}{4} + \frac{(\mathrm{Mc}^2+E_{\mathrm{nk}}-C_s)\sigma^2 D}{\alpha^2\hbar^2c^2} + \frac{k(k+1)}{4\alpha^2 r_e^2}C_2} - n - \frac{1}{2}}\right)^2,
\end{aligned} \tag{11}$$

where $n = 0, 1, 2, \ldots n_{\max}$. In this context, the coefficients $C_0$, $C_1$, and $C_2$ are explicitly determined as

$$\begin{aligned}
C_0 &= A_0 + A_1 + A_2 = 1 - \left(\frac{1 + e^{-2\alpha r_e}}{2\alpha r_e}\right)^2\left[\frac{8\alpha r_e}{1 + e^{-2\alpha r_e}} - 3 - 2\alpha r_e\right], \\
C_1 &= 2A_1 + 4A_2 = -\left(1 + e^{2\alpha r_e}\right)\cdot\frac{1 + e^{-2\alpha r_e}}{2\alpha r_e}\left[3 - (3 + 2\alpha r_e)\left(\frac{1 + e^{-2\alpha r_e}}{2\alpha r_e}\right)\right], \\
C_2 &= 4A_2 = \left(1 + e^{2\alpha r_e}\right)^2\left(\frac{1 + e^{-2\alpha r_e}}{2\alpha r_e}\right)^2\left[3 + 2\alpha r_e - \frac{4\alpha r_e}{1 + e^{-2\alpha r_e}}\right].
\end{aligned} \tag{12}$$

**vii)** Next, we elucidate the energy spectrum equation derived from the GTHP with parameters $V_1 = P_1 + \frac{P_2}{2} + \frac{P_3}{4}$, $V_2 = -\frac{P_2}{2} - \frac{P_3}{2}$, and $V_3 = \frac{P_3}{4}$ for the four-parameter exponential-type potential. This culminates in:

$$\begin{aligned}
&\left(\mathrm{Mc}^2 - C_s\right)^2 - E_{\mathrm{nk}}^2 + \left(\mathrm{Mc}^2 + E_{\mathrm{nk}} - C_s\right)P_1 + \frac{\hbar^2 c^2 k(k+1)}{r_e^2}(A_0 + A_1 + A_2) \\
&= \alpha^2\hbar^2c^2\left(\sqrt{\frac{1}{4} + \frac{(\mathrm{Mc}^2 + E_{\mathrm{nk}} - C_s)P_3}{4\alpha^2\hbar^2c^2} + \frac{k(k+1)}{\alpha^2 r_e^2}A_2}\right.
\end{aligned}$$

$$-n-\frac{1}{2}-\frac{\frac{(\mathrm{Mc}^2+E_{\mathrm{nk}}-C_s)(P_2+P_3)}{4\alpha^2\hbar^2c^2}-\frac{k(k+1)}{2\alpha^2r_e^2}A_1}{\sqrt{\frac{1}{4}+\frac{(\mathrm{Mc}^2+E_{\mathrm{nk}}-C_s)P_3}{4\alpha^2\hbar^2c^2}+\frac{k(k+1)}{\alpha^2r_e^2}A_2}-n-\frac{1}{2}}\Bigg)^2. \tag{13}$$

The quantum number range is again specified by $n = 0, 1, 2, \ldots, n_{\max}$.

**viii)** The parameters for the GTHP, designated as $V_1$, $V_2$, and $V_3$, are defined, respectively, by the relations $V_1 = \frac{W_1+W_2+W_3}{4}$, $V_2 = \frac{W_3-W_1}{2}$, and $V_3 = \frac{W_1-W_2+W_3}{4}$. These parameters are instrumental in deriving the energy spectrum equation for the Williams–Poulios type-potential. By substituting these definitions, the equation governing the energy spectrum can be expressed as follows:

$$\begin{aligned}&\left(\mathrm{Mc}^2-C_s\right)^2-E_{\mathrm{nk}}^2+\left(\mathrm{Mc}^2+E_{\mathrm{nk}}-C_s\right)W_3+\frac{\hbar^2c^2k(k+1)}{r_e^2}(A_0+A_1+A_2)\\&=\alpha^2\hbar^2c^2\Bigg(\sqrt{\frac{1}{4}+\frac{(\mathrm{Mc}^2+E_{\mathrm{nk}}-C_s)(W_1-W_2+W_3)}{4\alpha^2\hbar^2c^2}+\frac{k(k+1)}{\alpha^2r_e^2}A_2}-n-\frac{1}{2}\\&-\frac{\frac{(\mathrm{Mc}^2+E_{\mathrm{nk}}-C_s)(W_1-W_3)}{4\alpha^2\hbar^2c^2}-\frac{k(k+1)}{2\alpha^2r_e^2}A_1}{\sqrt{\frac{1}{4}+\frac{(\mathrm{Mc}^2+E_{\mathrm{nk}}-C_s)(W_1-W_2+W_3)}{4\alpha^2\hbar^2c^2}+\frac{k(k+1)}{\alpha^2r_e^2}A_2}-n-\frac{1}{2}}\Bigg)^2.\end{aligned} \tag{14}$$

This equation is valid for quantum numbers $n = 0, 1, 2, \ldots, n_{\max}$.

**ix)** In the regime where $\alpha$ is significantly smaller than unity, the energy levels as described by Eq. (3) simplify to:

$$\begin{aligned}&\left(\mathrm{Mc}^2-C_s\right)^2-E_{\mathrm{nk}}^2+\left(V_1-\frac{V_2^2}{4V_3}\right)(\mathrm{Mc}^2+E_{\mathrm{nk}}-C_s)\\&+\frac{\hbar^2c^2k(k+1)}{r_e^2}+2\alpha\hbar c\left(1-\frac{V_2^2}{4V_3^2}\right)\sqrt{(\mathrm{Mc}^2+E_{\mathrm{nk}}-C_s)V_3}\\&\times\left(n+\frac{1}{2}\right)-\alpha^2\hbar^2c^2\left[\left(1+\frac{3V_2^2}{4V_3^2}\right)\left(n+\frac{1}{2}\right)^2+\frac{1}{4}\left(1-\frac{V_2^2}{4V_3^2}\right)\right]+o\left(\alpha^2\right)=0.\end{aligned} \tag{15}$$

This approximation holds for small values of $n$ and $l$.

**x)** Setting $C_s = 0$ allows us to simplify the potential for the energy level equation of a Klein-Gordon particle, resulting in Ref. [44]:

$$\begin{aligned}&E_{\mathrm{nk}}^2-M^2c^4-\left(\mathrm{Mc}^2+E_{\mathrm{nk}}\right)(V_1+V_2+V_3)-\frac{\hbar^2c^2l(l+1)}{r_e^2}(A_0+A_1+A_2)\\&+\alpha^2\hbar^2c^2\Bigg(\sqrt{\frac{1}{4}+\frac{(\mathrm{Mc}^2+E_{\mathrm{nk}})V_3}{\alpha^2\hbar^2c^2}+\frac{l(l+1)}{\alpha^2r_e^2}A_2}-n-\frac{1}{2}\\&+\frac{\frac{(\mathrm{Mc}^2+E_{\mathrm{nk}})V_2}{2\alpha^2\hbar^2c^2}+\frac{l(l+1)}{2\alpha^2r_e^2}A_1}{\sqrt{\frac{1}{4}+\frac{(\mathrm{Mc}^2+E_{\mathrm{nk}})V_3}{\alpha^2\hbar^2c^2}+\frac{l(l+1)}{\alpha^2r_e^2}A_2}-n-\frac{1}{2}}\Bigg)^2=0.\end{aligned} \tag{16}$$

Applicable for $n = 0, 1, 2, \ldots, n_{\max}$.

**xi)** Finally, applying the transformations $E_{\mathrm{nk}} - \mathrm{Mc}^2 + C_s \to E_{\mathrm{nl}}$ and $E_{\mathrm{nk}} + \mathrm{Mc}^2 - C_s \to 2\mu c^2$ to Eq. (3), we derive the energy spectrum for the non-relativistic scenario:

$$\begin{aligned}E_{\mathrm{nl}}=&(V_1+V_2+V_3)+\frac{\hbar^2c^2l(l+1)}{2\mu r_e^2}(A_0+A_1+A_2)\\&-\frac{\alpha^2\hbar^2}{2\mu}\Bigg[\sqrt{\frac{1}{4}+\frac{2\mu V_3}{\alpha^2\hbar^2}+\frac{l(l+1)}{\alpha^2r_e^2}A_2}-n-\frac{1}{2}\\&+\frac{\frac{\mu V_2}{\alpha^2\hbar^2}+\frac{l(l+1)}{2\alpha^2r_e^2}A_1}{\sqrt{\frac{1}{4}+\frac{2\mu V_3}{\alpha^2\hbar^2}+\frac{l(l+1)}{\alpha^2r_e^2}A_2}-n-\frac{1}{2}}\Bigg]^2.\end{aligned} \tag{17}$$

This formulation aligns with the findings presented in Ref. [43], valid for $n = 0, 1, 2, \ldots, n_{\max}$.

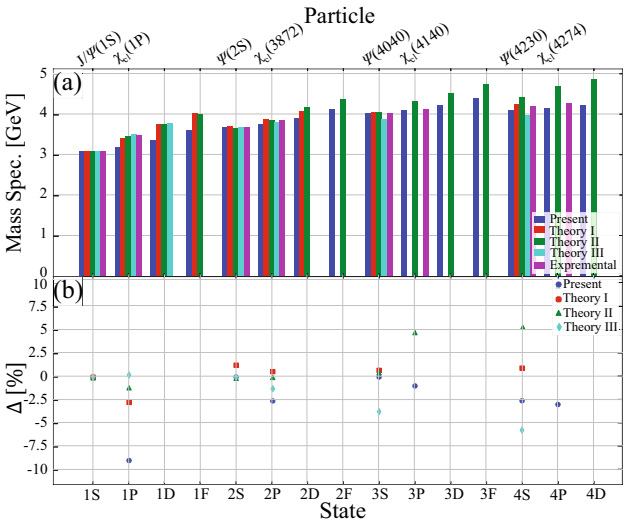


**Fig. 1** **a** Non-relativistic calculating mass spectra of charmonium $M_{c\bar{c}}$ in GeV for $m_c = 1.27$ GeV; $V_1 = 7.404662$ GeV; $V_2 = -20.779639$ GeV; $V_3 = 14.959636$ GeV; $\alpha = 0.223612$ GeV; $r_e = 3.830931$ GeV$^{-1}$. The experimental data from Ref. [75] and other theoretical predictions: Theory I from Ref. [61], Theory II from Ref. [62], Theory III from Ref. [63] are also included for comparison. **b** Corresponding deviations from the experimental data

Briefly, in the spin symmetry, the GTHP's inclusion of Woods–Saxon and Morse potentials means it can be used in nuclear bound-state problems (like nucleon–nucleus potential models) or molecular/atomic systems that employ Morse-type interactions. However, an equally important spin symmetry, pseudo-spin symmetry, also plays a crucial role in relativistic quantum systems [18, 19]. Pseudo-spin symmetry arises when the sum of the vector and scalar potentials satisfies $V(r) + S(r) =$ constant [18, 19]. This symmetry is closely related to the near-degeneracy of nuclear energy levels and offers a complementary perspective to the spin symmetry analysis [25, 26]. The investigation of pseudo-spin symmetry is vital for understanding nuclear shell structures, meson spectroscopy, and the underlying physics governing quark–antiquark pairs [27–37]. Therefore, we extend our analysis to pseudo-spin symmetry within the GTHP framework, examining its manifestation across different potential profiles and its impact on the system's energy spectrum in the Section S2 of Ref. [79]. This transition from spin symmetry to pseudo-spin symmetry reinforces the unified nature of these symmetries and their relevance to nuclear and particle physics.

### 3.2 Analysis of charmonium and bottomonium mass spectra

In this part, we mainly focus on the non-relativistic modeling of charmonium and bottomonium systems (See detailed modeling information in S3.A section in Ref. [79]), as it exhibits better agreement with experimental data across both low- and high-energy states. The following analysis delves into specific comparisons and explores the underlying physical implications of these findings.

The calculated charmonium mass spectrum, as depicted in Fig. 1 and detailed in Table 1 and Table S1 in Ref. [79], shows a well agreement with experimental results, particularly for the $1S$ ($J/\psi(1S)$), $2S$ ($\psi(2S)$), and $3S$ ($\psi(4040)$) states. Notably, the $J/\psi(1S)$ state matches precisely at 3.096900 GeV, underscoring the efficacy of the GTHP model in predicting ground state masses where non-relativistic approximations hold strong.

However, the model's performance varies across different orbital states. While $S$-wave states are well-described, higher orbital states, such as the $1P$ ($\chi_{c1}(1P)$) state, exhibit deviations of $-8.96\%$ (see Fig. 1a) for non-relativistic case, respectively. Such discrepancies indicate the need for further refinement in modeling higher orbital angular momentum states. The significant deviations observed in these states suggest that the influence of relativistic effects, spin-orbit coupling, and other acceptable structure corrections become more pronounced. Again, in our context of relativistic treatment, using the Eq. (3), we observe relatively larger deviations from experimental data, especially in the $1P$ and other higher orbital states, primarily due to the overestimation of relativistic contributions without proper spin-orbit interaction corrections.

Another reason for the observed deviations can be that the analytic heavy- $Q\bar{Q}$ potential behaves like a Coulomb+linear ("Cornell") potential at short distances but flattens at large $r$, thereby mimicking QCD string breaking. Figure 2 compares the GTHP (solid curve) to a conventional linear confining potential. At large separations the GTHP flattens, reflecting the string-breaking screening expected in full QCD [85–89]. In practice this means that beyond roughly $r \sim$ 1.0-1.2 fm the effective confining force weakens (approaching the threshold of two non-interacting heavy-light mesons [88]). Consequently, compact $S$-wave quarkonia (with small radii) reside almost entirely within the steep central region of the potential and are well-described by the model. By contrast, $P$-wave states have larger spatial extent and sample the softened tail of the potential; since the confining strength is weaker at these distances, the predicted $P$-wave binding is insufficient. This under-binding of the $P$-waves is therefore a natural consequence of the screened potential choice. Lattice QCD results confirm that the static heavy quark potential saturates at long range due to light-quark pair creation [86, 88]. We conclude that while the GTHP provides an accurate description of the compact $S$-states, further refinements (e.g., additional interaction terms or coupled-channel effects) will be required to capture the physics of the more extended $P$-wave states.

**Table 1** Mass spectra of charmonium $M_{c\bar{c}}$ in GeV for $m_c = 1.27$ GeV; $V_1 = 7.404662$ GeV; $V_2 = -20.779639$ GeV; $V_3 = 14.959636$ GeV; $\alpha = 0.223612$ GeV; $r_e = 3.830931$ GeV$^{-1}$. The percentage deviation from experimental values is presented below each calculated value

| State | Particle | Present Work Non-Rel. | Theory I Ref. [61] | Theory II Ref. [62] | Theory III Ref. [63] | Experiment Ref. [75] |
|---|---|---|---|---|---|---|
| 1S | J/$\psi$(1S) | 3.096900 | 3.096 | 3.094 | 3.0969 | 3.09690 |
| | | 0.00% | −0.03% | −0.09% | 0.00% | |
| 1P | $\chi_{c1}$(1P) | 3.196126 | 3.415 | 3.468 | 3.518 | 3.51067 |
| | | −8.96% | −2.71% | −1.22% | 0.21% | |
| 1D | – | 3.377174 | 3.770 | 3.772 | 3.787 | 3.77370 |
| 1F | – | 3.617957 | 4.040 | 4.012 | – | – |
| 2S | $\psi$(2S) | 3.686100 | 3.733 | 3.681 | 3.686 | 3.68610 |
| | | 0.00% | 1.27% | −0.14% | 0.00% | |
| 2P | $\chi_{c1}$(3872) | 3.772214 | 3.894 | 3.938 | 3.823 | 3.87165 |
| | | −2.57% | 0.58% | 1.71% | −1.26% | |
| 2D | – | 3.930322 | 4.088 | 4.188 | – | – |
| 2F | – | 4.143411 | – | 4.396 | – | – |
| 3S | $\psi$(4040) | 4.039000 | 4.068 | 4.129 | 3.889 | 4.03900 |
| | | 0.00% | 0.72% | 2.23% | −3.71% | |
| 3P | $\chi_{c1}$(4140) | 4.106798 | – | 4.338 | – | 4.14650 |
| | | −0.96% | | 4.62% | | |
| 3D | – | 4.233365 | – | 4.557 | – | – |
| 3F | – | 4.409120 | – | 4.746 | – | – |
| 4S | $\psi$(4230) | 4.115000 | 4.263 | 4.514 | 3.982 | 4.22270 |
| | | −2.55% | 0.95% | 6.90% | −5.70% | |
| 4P | $\chi_{c1}$(4274) | 4.159579 | – | 4.696 | – | 4.28600 |
| | | −2.95% | | 9.57% | | |
| 4D | – | 4.246829 | – | 4.896 | – | – |

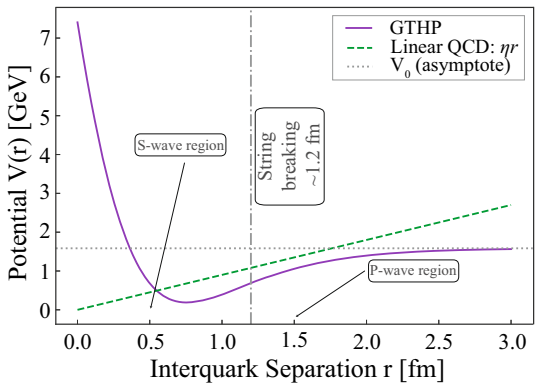


**Fig. 2** Comparison between the GTHP potential (solid) and a linear confinement potential (dashed). The GTHP realistically captures QCD string breaking by saturating at large distances, accurately describing compact *S*-wave states but reducing confinement for extended *P*-wave states [85–88]

In order to remove these discrepancies, spin symmetry breaking can be introduced through the parameter $C_s$, which allows for fine-tuning to match the ground state with experimental values. Although this improved the overall agreement, particularly for the charmonium system, the deviations for higher angular momentum states persisted. This is due to the fact that Eq. (3) are obtained for spin symmetry case. The interaction potential may need to be adjusted to account for quark–antiquark dynamics more comprehensively, particularly in exact spin-orbit correction that naturally arise in systems with non-negligible quark masses. To gain further improvements in the relativistic model, one has to go to higher order corrections like refined GTHP with Tensor potentials or solve two body DE and Bethe–Salpeter formalism with GTHP, as these methods account more accurately for spin-dependent interactions in higher excited states. For a detailed exploration of the relativistic mass spectra and a comprehensive comparison between non-relativistic and relativistic results with the full set of mass spectra tables, analysis of spin symmetry breaking, readers can be found in section S3.B of Ref. [79].

For bottomonium, the mass spectra shown in Fig. 3 and detailed in Table 2 and also Table S2 in Ref. [79] reveal an even closer agreement with experimental data, particularly for the 1S ($\Upsilon$(1S)), 2S ($\Upsilon$(2S)), and 3S ($\Upsilon$(3S)) states, where deviations from experimental values are around 0.0%, see Fig. 3. This demonstrates the robustness of the GTHP model in predicting bottomonium states, where the non-relativistic approximation is more justified due to the larger bottom quark mass. For higher states, such as the 1P (hb(1P)), 1D ($\Upsilon$2(1D)), 2P (hb(2P)), and 4S ($\Upsilon$(4S)) states, the deviations are slightly more significant, ranging from -1.06% to

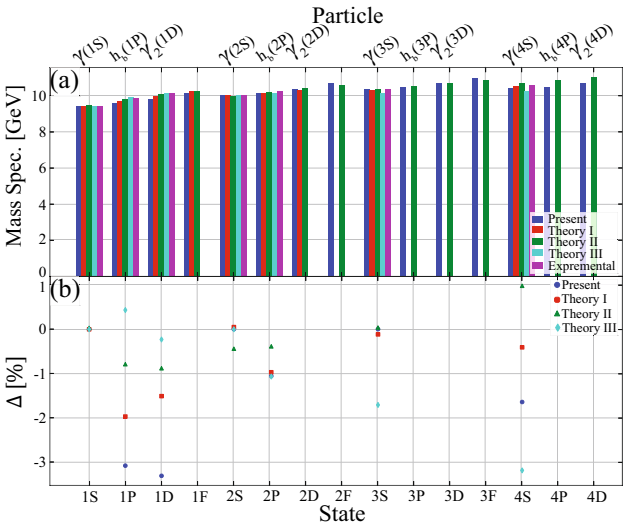


**Fig. 3** Non-relativistic calculating mass spectra of bottomonium $M_{b\bar{b}}$ in GeV for $m_b = 4.18$ GeV; $V_1 = 4.883229$ GeV; $V_2 = -12.928267$ GeV; $V_3 = 10.108982$ GeV; $\alpha = 0.412272$ GeV; $r_e = 1.836733$ GeV$^{-1}$. The experimental data from Ref. [75] and other theoretical predictions: Theory I from Ref. [61], Theory II from Ref. [62], Theory III from Ref. [63] are also included for comparison. **b** Corresponding deviations from the experimental data

**Table 2** Mass spectra of bottomonium $M_{b\bar{b}}$ in GeV for $m_b = 4.18$ GeV; $V_1 = 4.883229$ GeV; $V_2 = -12.928267$ GeV; $V_3 = 10.108982$ GeV; $\alpha = 0.412272$ GeV; $r_e = 1.836733$ GeV$^{-1}$. The percentage deviation from experimental values is presented below each calculated value

| State | Particle | Present Work Non-Rel. | Theory I Ref. [61] | Theory II Ref. [62] | Theory III Ref. [63] | Experiment Ref. [75] |
|---|---|---|---|---|---|---|
| 1S | $\Upsilon(1S)$ | 9.460302 | 9.460 | 9.463 | 9.460 | 9.46030 |
| | | 0.00% | 0.00% | 0.03% | 0.00% | |
| 1P | $h_b(1P)$ | 9.594182 | 9.704 | 9.821 | 9.942 | 9.8993 |
| | | −3.08% | −1.97% | −0.79% | 0.43% | |
| 1D | $\Upsilon_2(1D)$ | 9.827113 | 10.010 | 10.074 | 10.140 | 10.1637 |
| | | −3.31% | −1.51% | −0.88% | −0.23% | |
| 1F | – | 10.130188 | 10.268 | 10.288 | – | – |
| 2S | $\Upsilon(2S)$ | 10.023261 | 10.028 | 9.979 | 10.023 | 10.02326 |
| | | 0.00% | 0.05% | −0.44% | 0.00% | |
| 2P | $h_b(2P)$ | 10.151214 | 10.160 | 10.220 | 10.150 | 10.2598 |
| | | −1.06% | −0.97% | −0.39% | −1.07% | |
| 2D | $\Upsilon_2(2D)$ | 10.380036 | 10.332 | 10.424 | – | – |
| 2F | – | 10.688957 | – | 10.607 | – | – |
| 3S | $\Upsilon(3S)$ | 10.355200 | 10.343 | 10.359 | 10.178 | 10.3552 |
| | | 0.00% | −0.12% | 0.04% | −1.71% | |
| 3P | $h_b(3P)$ | 10.468567 | – | 10.556 | – | – |
| 3D | $\Upsilon_2(3D)$ | 10.681781 | – | 10.733 | – | – |
| 3F | – | 10.986923 | – | 10.897 | – | – |
| 4S | $\Upsilon(4S)$ | 10.405400 | 10.536 | 10.683 | 10.242 | 10.5794 |
| | | −1.64% | −0.41% | 0.98% | −3.18% | |
| 4P | $h_b(4P)$ | 10.497089 | – | 10.855 | – | – |
| 4D | $\Upsilon_2(4D)$ | 10.686643 | – | 11.015 | – | – |

3.31% (see Fig. 3(b)). These minor discrepancies indicate that while the GTHP model is highly reliable even for excited states, there is room for improvement by incorporating relativistic and spin-orbital corrections. The model's accuracy in these states implies that the essential physics of quark confinement and interaction potentials are well captured. However, spin-spin, spin-orbit, and tensor interactions might need finer adjustments for higher precision.

While the GTHP model demonstrates good performance across a range of quantum states, a comparison with other theoretical models as Theory I (non-relativistic analyses of the linear plus modified Yukawa potential) [61], Theory II (non-relativistic analyses of quark-antiquark Cornell potential) [62], and Theory III (non-relativistic analyses of Cornell potential) [63]-reveals varying degrees of agreement. Although Theory II and III show closer results for lower energy states, the GTHP model provides better accuracy overall, especially for higher orbital states. This indicates that the GTHP has provided a more powerful description of quarkonium systems, especially in the high-energy region. Also, our non-relativistic quantummechanical treatment yields important insights, especially in the lower-energy region, but we have to be aware of its limitations when considering higher orbital states or systems

with significant relativistic effects. This framework includes spin effects semi-inclusively, but a completely relativistic treatment will necessitate in addition the formulation and solution of two-body DE [90–92] as well as the Bethe-Salpeter equation [93]. Implicitly in this approach would be the relativistic corrections our model now "corrects", providing a more realistic picture of quarkantiquark dynamics, especially regarding higher angularmomentum states. Note that a relativistic treatment could entail more than just this pair term – in particular, we might have important correlations through spin-orbit coupling, which are known to induce fine structure splittings not accounted for by our model [75].

Such the two-body DE [90–92] and the Bethe-Salpeter equation [66, 93] formalism can also open avenues with GTHP for exploring new quarkonium states that may emerge owing to relativistic effects, which are not predicted by conventional non-relativistic models. These heavily bound states may include, e.g., the very tightlybound ones with large binding energies where tests of the model can be made against experiments; and new states which are created under extremely severe conditions in such things as a heavy-ion collision plasma situations where non-relativistic models might be insufficient. The predictions by this model of possible new states with longevity at extreme conditions can also be significant in the context of heavy-ion collisions, where quark-gluon plasma might be created and where new bound states might be discovered. Expanding this framework and applying it to mixed-flavor systems like bottom-charm (Bc) mesons can also yield deeper insights into quark confinement and the dynamics of the strong force. Such predictions, although speculative, highlight the need for closing elliptical states not only in the GTHP model but also by including more sophisticated interactions to study a whole range of quarkonium states. Given these, while hardy in its current form, the GTHP model may serve as a starting block for more advanced models. A more accurate treatment together with incorporating more complex interactions will enable a deeper study of quarkonium states and give us access to a wider domain of the strong interactions that are responsible for these configurations.

## 4 Conclusions

In this study, we derived the analytical solution of the DE in the context of spin and pseudo-spin symmetries for the GTHP by using NU method and demonstrated its effectiveness in reproducing the mass spectra of charmonium and bottomonium with sufficient accuracy. The flexibility of the GTHP allows its application in different quantum systems, potentially holding its place in our approach to solving complex fermionic systems. For the analysis of the mass spectra of charmonium and bottomonium, our findings for the low $S$-wave states, namely $J/\psi(1\,S)$, $\psi(2\,S)$ and $\psi(4040)$, were in good agreement with the reported experimental data. This finding emphasized the accuracy of the model in the non-relativistic regime, especially for heavy quark systems such as bottomonium, where deviations from experimental masses are minimal. However, in the higher orbital states, such as $1P \longmapsto 4P$ ($\chi_{c1}$) for charmonium and $1P$ ($h_b(1P)$) and $1D$ ($\Upsilon_2(1D)$) for bottomonium, we observed the relatively larger discrepancy. While the non-relativistic analyses of the GTHP model adequately capture the fundamental dynamics of the heavy quarkonium, it was also shown that the inclusion of relativistic and spin-dependent effects is necessary to advance the description of higher orbital states. For systems with more than one flavor species, such as $B_c$ mesons, a corresponding formulation taking spin-orbit corrections into account can shed more light on the propagation of aberrations owing to quark confinement and the strong force. Its overall performance provided a strong basis for theoretical considerations and reliable predictions with significant potential for further development.

**Supplementary Information** The online version contains supplementary material available at https://doi.org/10.1140/epjp/s13360-025-06630-4.

**Acknowledgements** We would like to acknowledge the invaluable contributions of our co-author, A. I. Ahmadov, to beginning of this work. We are deeply saddened by his passing and honor his memory through this publication.

**Funding** Open Access funding enabled and organized by Projekt DEAL.

**Data Availability Statement** All data that support the findings of this study are included within the article (and any supplementary files).

**Declarations**

**Conflict of interest** The authors declare no Conflict of interest. All research has been carried out within an appropriate ethical framework.



## References

1. P. Dirac, N. Bohr, Proc. R. Soc. Lond. A **114**, 243 (1927). https://doi.org/10.1098/rspa.1927.0039
2. P. Dirac, J. Math. Phys. **4**, 901 (1963). https://doi.org/10.1063/1.1704016

3. H. Feshbach, F. Villars, Rev. Mod. Phys. **30**, 24 (1958). https://doi.org/10.1103/RevModPhys.30.24
4. P. Dirac, Rev. Mod. Phys. **21**, 392 (1949). https://doi.org/10.1103/RevModPhys.21.392
5. B.H. Chirgwin, H.T. Flint, Nature **155**, 724 (1945). https://doi.org/10.1038/155724a0
6. S.A. Giuliani, Z. Matheson, W. Nazarewicz, E. Olsen, P.-G. Reinhard, J. Sadhukhan, B. Schuetrumpf, N. Schunck, P. Schwerdtfeger, Rev. Mod. Phys. **91**, 011001 (2019). https://doi.org/10.1103/RevModPhys.91.011001
7. N. Li, M. Shi, J.-Y. Guo, Z.-M. Niu, H. Liang, Phys. Rev. Lett. **117**, 062502 (2016). https://doi.org/10.1103/PhysRevLett.117.062502
8. H.-T. Ding, S.-T. Li, S. Mukherjee, A. Tomiya, X.-D. Wang, Y. Zhang, Phys. Rev. Lett. **126**, 082001 (2021). https://doi.org/10.1103/PhysRevLett.126.082001
9. A. Agarwal, Phys. Rev. Lett. **123**, 211601 (2019). https://doi.org/10.1103/PhysRevLett.123.211601
10. S.M. Barnett, Phys. Rev. Lett. **118**, 114802 (2017). https://doi.org/10.1103/PhysRevLett.118.114802
11. A.G. Campos, R. Cabrera, H.A. Rabitz, D.I. Bondar, Phys. Rev. Lett. **119**, 173203 (2017). https://doi.org/10.1103/PhysRevLett.119.173203
12. I. Bialynicki-Birula, Phys. Rev. Lett. **93**, 020402 (2004). https://doi.org/10.1103/PhysRevLett.93.020402
13. I. Kaminer, J. Nemirovsky, M. Rechtsman, R. Bekenstein, M. Segev, Nat. Phys. **11**, 261 (2015). https://doi.org/10.1038/nphys3196
14. F. Hammad, M. Simard, R. Saadati, A. Landry, Phys. Rev. D **110**, 065005 (2024). https://doi.org/10.1103/PhysRevD.110.065005
15. I. Bialynicki-Birula, Phys. Rev. D **103**, 085001 (2021). https://doi.org/10.1103/PhysRevD.103.085001
16. A. Mishra, A. Kumar, S.P. Misra, Phys. Rev. D **110**, 014003 (2024). https://doi.org/10.1103/PhysRevD.110.014003
17. P. Alberto, M. Fiolhais, M. Malheiro, A. Delfino, M. Chiapparini, Phys. Rev. Lett. **86**, 5015 (2001). https://doi.org/10.1103/PhysRevLett.86.5015
18. J.N. Ginocchio, Phys. Rev. Lett. **78**, 436 (1997). https://doi.org/10.1103/PhysRevLett.78.436
19. J.N. Ginocchio, Phys. Rep. **315**, 231 (1999). https://doi.org/10.1016/S0370-1573(99)00021-6
20. J.N. Ginocchio, Phys. Rev. C **69**, 034318 (2004). https://doi.org/10.1103/PhysRevC.69.034318
21. J.N. Ginocchio, Phys. Rep. **414**, 165 (2005). https://doi.org/10.1016/j.physrep.2005.04.003
22. H. Liang, J. Meng, S.-G. Zhou, Phys. Rep. **570**, 1 (2015). https://doi.org/10.1016/j.physrep.2014.12.005
23. S.-G. Zhou, J. Meng, P. Ring, Phys. Rev. Lett. **91**, 262501 (2003). https://doi.org/10.1103/PhysRevLett.91.262501
24. P.R. Page, T. Goldman, J.N. Ginocchio, Phys. Rev. Lett. **86**, 204 (2001). https://doi.org/10.1103/PhysRevLett.86.204
25. A. Arima, M. Harvey, K. Shimizu, Phys. Lett. B **30**, 517 (1969). https://doi.org/10.1016/0370-2693(69)90443-2
26. K. Hecht, A. Adler, Nucl. Phys. A **137**, 129 (1969). https://doi.org/10.1016/0375-9474(69)90077-3
27. M. de Voigt, J. Dudek, Z. Szymański, Rev. Mod. Phys. **55**, 949 (1983). https://doi.org/10.1103/RevModPhys.55.949
28. J. Dudek, W. Nazarewicz, Z. Szymanski, G.A. Leander, Phys. Rev. Lett. **59**, 1405 (1987). https://doi.org/10.1103/PhysRevLett.59.1405
29. W. Nazarewicz, P.J. Twin, P. Fallon, J.D. Garrett, Phys. Rev. Lett. **64**, 1654 (1990). https://doi.org/10.1103/PhysRevLett.64.1654
30. J.Y. Zeng, J. Meng, C.S. Wu, E.G. Zhao, Z. Xing, X.Q. Chen, Phys. Rev. C **44**, R1745 (1991). https://doi.org/10.1103/PhysRevC.44.R1745
31. T. Byrski, F.A. Beck, D. Curien, C. Schuck, P. Fallon, A. Alderson, I. Ali, M.A. Bentley, A.M. Bruce, P.D. Forsyth, D. Howe, J.W. Roberts, J.F. Sharpey-Schafer, G. Smith, P.J. Twin, Phys. Rev. Lett. **64**, 1650 (1990). https://doi.org/10.1103/PhysRevLett.64.1650
32. D. Troltenier, W. Nazarewicz, Z. Szymański, J. Draayer, Nucl. Phys. A **567**, 591 (1994). https://doi.org/10.1016/0375-9474(94)90026-4
33. A.E. Stuchbery, Nucl. Phys. A **700**, 83 (2002). https://doi.org/10.1016/S0375-9474(01)01300-8
34. Y. Nagai, J. Styczen, M. Piiparinen, P. Kleinheinz, D. Bazzacco, P.V. Brentano, K.O. Zell, J. Blomqvist, Phys. Rev. Lett. **47**, 1259 (1981). https://doi.org/10.1103/PhysRevLett.47.1259
35. L. Gaudefroy, O. Sorlin, D. Beaumel, Y. Blumenfeld, Z. Dombrádi, S. Fortier, S. Franchoo, M. Gélin, J. Gibelin, S. Grévy, F. Hammache, F. Ibrahim, K.W. Kemper, K.-L. Kratz, S.M. Lukyanov, C. Monrozeau, L. Nalpas, F. Nowacki, A.N. Ostrowski, T. Otsuka, Y.-E. Penionzhkevich, J. Piekarewicz, E.C. Pollacco, P. Roussel-Chomaz, E. Rich, J.A. Scarpaci, M.G. St, D. Laurent, M. Sohler, T. Stanoiu, E. Suzuki, D.V. Tryggestad, Phys. Rev. Lett. **97**, 092501 (2006). https://doi.org/10.1103/PhysRevLett.97.092501
36. B. Bastin, S. Grévy, D. Sohler, O. Sorlin, Z. Dombrádi, N.L. Achouri, J.C. Angélique, F. Azaiez, D. Baiborodin, R. Borcea, C. Bourgeois, A. Buta, A. Bürger, R. Chapman, J.C. Dalouzy, Z. Dlouhy, A. Drouard, Z. Elekes, S. Franchoo, S. Iacob, B. Laurent, M. Lazar, X. Liang, E. Liénard, J. Mrazek, L. Nalpas, F. Negoita, N.A. Orr, Y. Penionzhkevich, Z. Podolyák, F. Pougheon, P. Roussel-Chomaz, M.G. Saint-Laurent, M. Stanoiu, I. Stefan, F. Nowacki, A. Poves, Phys. Rev. Lett. **99**, 022503 (2007). https://doi.org/10.1103/PhysRevLett.99.022503
37. D. Troltenier, C. Bahri, J. Draayer, Nucl. Phys. A **586**, 53 (1995). https://doi.org/10.1016/0375-9474(94)00518-R
38. A.I. Ahmadov, S.M. Nagiyev, C. Aydin, V.A. Tarverdiyeva, M.S. Orujova, S.V. Badalov, Eur. Phys. J. Plus **137**, 1075 (2022). https://doi.org/10.1140/epjp/s13360-022-03255-9
39. A.S. de Castro, P. Alberto, Phys. Rev. A **86**, 032122 (2012). https://doi.org/10.1103/PhysRevA.86.032122
40. X.-D. Xu, S.-S. Zhang, A.J. Signoracci, M.S. Smith, Z.P. Li, Phys. Rev. C **92**, 024324 (2015). https://doi.org/10.1103/PhysRevC.92.024324
41. Z. Fang, M. Shi, J.-Y. Guo, Z.-M. Niu, H. Liang, S.-S. Zhang, Phys. Rev. C **95**, 024311 (2017). https://doi.org/10.1103/PhysRevC.95.024311
42. R.R. Hartmann, M.E. Portnoi, Phys. Rev. A **89**, 012101 (2014). https://doi.org/10.1103/PhysRevA.89.012101
43. H.I. Ahmadov, E.A. Dadashov, N.S. Huseynova, V.H. Badalov, Eur. Phys. J. Plus **136**, 244 (2021). https://doi.org/10.1140/epjp/s13360-021-01202-8
44. V.H. Badalov, S.V. Badalov, Commun. Theor. Phys. **75**, 075003 (2023). https://doi.org/10.1088/1572-9494/acd441
45. R.D. Woods, D.S. Saxon, Phys. Rev. **95**, 577 (1954). https://doi.org/10.1103/PhysRev.95.577
46. V.H. Badalov, B. Baris, K. Uzun, Mod. Phys. Lett. A **34**, 1950107 (2019). https://doi.org/10.1142/S0217732319501074
47. N. Rosen, P.M. Morse, Phys. Rev. **42**, 210 (1932). https://doi.org/10.1103/PhysRev.42.210
48. M.F. Manning, N. Rosen, Phys. Rev. **44**, 951 (1933). https://doi.org/10.1103/PhysRev.44.951
49. P.M. Morse, Phys. Rev. **34**, 57 (1929). https://doi.org/10.1103/PhysRev.34.57
50. C.-S. Jia, Y.-F. Diao, X.-J. Liu, P.-Q. Wang, J.-Y. Liu, G.-D. Zhang, J. Chem. Phys. **137**, 014101 (2012). https://doi.org/10.1063/1.4731340
51. D. Schiöberg, Mol. Phys. **59**, 1123 (1986). https://doi.org/10.1080/00268978600102631
52. P.-Q. Wang, L.-H. Zhang, C.-S. Jia, J.-Y. Liu, J. Mol. Spectr. **274**, 5 (2012). https://doi.org/10.1016/j.jms.2012.03.005
53. J. Chun-Sheng, Z. Ying, Z. Xiang-Lin, S. Liang-Tian, Commun. Theor. Phys. **36**, 641 (2001). https://doi.org/10.1088/0253-6102/36/6/641
54. A.N. Ikot, B.C. Lutfuoglu, M.I. Ngwueke, M.E. Udoh, S. Zare, H. Hassanabadi, Eur. Phys. J. Plus **131**, 419 (2016). https://doi.org/10.1140/epjp/i2016-16419-5
55. B.W. Williams, D.P. Poulios, Eur. J. Phys. **14**, 222 (1993). https://doi.org/10.1088/0143-0807/14/5/006
56. J.J. Peña, J. Morales, J. García-Ravelo, J. Math. Phys. **58**, 043501 (2017). https://doi.org/10.1063/1.4979617
57. J. Soto, S. Tomàs Valls, Phys. Rev. D **108**, 014025 (2023). https://doi.org/10.1103/PhysRevD.108.014025
58. B. Patel, P.C. Vinodkumar, J. Phys. G: Nucl. Part. Phys. **36**, 035003 (2009). https://doi.org/10.1088/0954-3899/36/3/035003
59. J. Sebastian, M.Y. Jamal, N. Haque, Phys. Rev. D **107**, 054040 (2023). https://doi.org/10.1103/PhysRevD.107.054040
60. N. Brambilla, A. Pineda, J. Soto, A. Vairo, Rev. Mod. Phys. **77**, 1423 (2005). https://doi.org/10.1103/RevModPhys.77.1423
61. K.R. Purohit, P. Jakhad, A.K. Rai, Phys. Scr. **97**, 044002 (2022). https://doi.org/10.1088/1402-4896/ac5bc2

62. N.R. Soni, B.R. Joshi, R.P. Shah, H.R. Chauhan, J.N. Randya, Eur. Phys. J. C **78**, 592 (2018). https://doi.org/10.1140/epjc/s10052-018-6068-6
63. B. Bukor, J. Tekel, Eur. Phys. J. Plus **138**, 499 (2023). https://doi.org/10.1140/epjp/s13360-023-04049-3
64. B.-Q. Li, K.-T. Chao, Phys. Rev. D **79**, 094004 (2009). https://doi.org/10.1103/PhysRevD.79.094004
65. R.-H. Ni, Q. Li, X.-H. Zhong, Phys. Rev. D **105**, 056006 (2022). https://doi.org/10.1103/PhysRevD.105.056006
66. D. Molina, M. De Sanctis, C. Fernández-Ramírez, Phys. Rev. D **95**, 094021 (2017). https://doi.org/10.1103/PhysRevD.95.094021
67. Q. Deng, R.-H. Ni, Q. Li, X.-H. Zhong, Phys. Rev. D **110**, 056034 (2024). https://doi.org/10.1103/PhysRevD.110.056034
68. E.J. Eichten, C. Quigg, Phys. Rev. D **52**, 1726 (1995). https://doi.org/10.1103/PhysRevD.52.1726
69. T. Kawanai, S. Sasaki, Phys. Rev. D **89**, 054507 (2014). https://doi.org/10.1103/PhysRevD.89.054507
70. S. Godfrey, N. Isgur, Phys. Rev. D **32**, 189 (1985). https://doi.org/10.1103/PhysRevD.32.189
71. C. Quigg, J.L. Rosner, Phys. Rep. **56**, 167 (1979). https://doi.org/10.1016/0370-1573(79)90095-4
72. N. Brambilla, S. Eidelman, B.K. Heltsley, R. Vogt, G.T. Bodwin, E. Eichten, A.D. Frawley, A.B. Meyer, R.E. Mitchell, V. Papadimitriou, P. Petreczky, A.A. Petrov, P. Robbe, A. Vairo, A. Andronic, R. Arnaldi, P. Artoisenet, G. Bali, A. Bertolin, D. Bettoni, J. Brodzicka, G.E. Bruno, A. Caldwell, J. Catmore, C.-H. Chang, K.-T. Chao, E. Chudakov, P. Cortese, P. Crochet, A. Drutskoy, U. Ellwanger, P. Faccioli, A. Gabareen Mokhtar, X. Garcia i Tormo, C. Hanhart, F.A. Harris, D.M. Kaplan, S.R. Klein, H. Kowalski, J.-P. Lansberg, E. Levichev, V. Lombardo, C. Lourenço, F. Maltoni, A. Mocsy, R. Mussa, F.S. Navarra, M. Negrini, M. Nielsen, S.L. Olsen, P. Pakhlov, G. Pakhlova, K. Peters, A.D. Polosa, W. Qian, J.-W. Qiu, G. Rong, M.A. Sanchis-Lozano, E. Scomparin, P. Senger, F. Simon, S. Stracka, Y. Sumino, M. Voloshin, C. Weiss, H. K. Wöhri, C.-Z. Yuan, Eur. Phys. J. C **71**, 1534 (2011). https://doi.org/10.1140/epjc/s10052-010-1534-9
73. E. Eichten, K. Gottfried, T. Kinoshita, K.D. Lane, T.M. Yan, Phys. Rev. D **17**, 3090 (1978). https://doi.org/10.1103/PhysRevD.17.3090
74. W.-L. Sang, D.-S. Yang, Y.-D. Zhang, Phys. Rev. D **108**, 014021 (2023). https://doi.org/10.1103/PhysRevD.108.014021
75. Particle Data Group, R.L. Workman, V.D. Burkert, et al., Prog. Theor. Exp. Phys. **2022**, 083C01 (2022)
76. S. Godfrey, K. Moats, Phys. Rev. D **92**, 054034 (2015). https://doi.org/10.1103/PhysRevD.92.054034
77. W. Greiner, *Quantum Mechanics: An Introduction*, 4th edn. (Springer, Berlin Heidelberg, 2001)
78. A.F. Nikiforov, V.B. Uvarov, Special Funct. Math. Phys. (1988). https://doi.org/10.1007/978-1-4757-1595-8
79. Additional details, theoretical derivations, and supplementary analyses can be found in the Supplementary Material, which also includes Ref. [21,22,43,44,61–63,75,77, 78] to support this study
80. D. Fioravanti, D. Gregori, Phys. Lett. B **804**, 135376 (2020). https://doi.org/10.1016/j.physletb.2020.135376
81. D. Fioravanti, M. Rossi, Phys. Lett. B **838**, 137706 (2023). https://doi.org/10.1016/j.physletb.2023.137706
82. D. Fioravanti, D. Gregori, From quasinormal modes to exact wkb quantization in ads black holes (2021), arXiv:abs/2112.11434
83. D. Fioravanti, D. Gregori, H. Shu, Exact quantization of scalar quasinormal modes in ads black holes via $\mathcal{N} = 2$ gauge theories (2022), arXiv:abs/2208.14031
84. H. Feizi, M.R. Shojaei, A.A. Rajabi, Eur. Phys. J. Plus **127**, 41 (2012). https://doi.org/10.1140/epjp/i2012-12041-y
85. N. Isgur, J. Paton, Phys. Rev. D **31**, 2910 (1985). https://doi.org/10.1103/PhysRevD.31.2910
86. G.S. Bali, Phys. Rep. **343**, 1 (2001). https://doi.org/10.1016/S0370-1573(00)00079-X
87. G.S. Bali, H. Neff, T. Düssel, T. Lippert, K. Schilling, Phys. Rev. D **71**, 114513 (2005). https://doi.org/10.1103/PhysRevD.71.114513
88. J. Bulava, B. Hörz, F. Knechtli, V. Koch, G. Moir, C. Morningstar, M. Peardon, Phys. Lett. B **793**, 493 (2019). https://doi.org/10.1016/j.physletb.2019.05.018
89. C. Bernard, T. Burch, T. DeGrand, C. DeTar, S. Gottlieb, U. Heller, P. Lacock, K. Orginos, R. Sugar, D. Toussaint, Nucl. Phys. B **94**, 546 (2001). https://doi.org/10.1016/S0920-5632(01)00863-5
90. H. W. Crater, J.-H. Yoon, and C.-Y. Wong, Phys. Rev. D **79**, 034011 (2009). https://doi.org/10.1103/PhysRevD.79.034011
91. T. C. Scott, J. Shertzer, and R. A. Moore, Phys. Rev. A **45**, 4393 (1992). https://doi.org/10.1103/PhysRevA.45.4393
92. P. L. Ferreira, Phys. Rev. D **38**, 2648 (1988). https://doi.org/10.1103/PhysRevD.38.2648
93. T. Hilger, C. Popovici, M. Gómez-Rocha, and A. Krassnigg, Phys. Rev. D **91**, 034013 (2015). https://doi.org/10.1103/PhysRevD.91.034013
94. C. L. Pekeris, Phys. Rev. **45**, 98 (1934). https://doi.org/10.1103/PhysRev.45.98
95. M. Abramowitz and I. A. Stegun, Handbook of Mathematical Functions with Formulas, Graphs, and Mathematical Tables (Dover Publications, New York, 2012).